Tellus (1995), 47A, 331–350
Printed in Belgium

TELLUS
ISSN 0280-6495

Interaction between the low- and high-frequency transients in the Southern Hemisphere winter circulation

By THOMAS J. CUFF and MING CAI*, *Cooperative Institute for Climate Studies, Department of Meteorology, University of Maryland, College Park, MD 20742, USA*

(Manuscript received 18 April 1994; in final form 28 August 1994)

ABSTRACT

A symbiotic relationship between the high- and low-frequency transients in the Southern Hemisphere has been examined by using ECMWF analyses of 500 mb geopotential height and temperature fields over 9 winter seasons. The low-frequency transients organize the high-frequency eddies over the regions where low-frequency westerly anomalies prevail, forming traveling storm tracks that move together with the low-frequency waves. The high-frequency eddies, in turn, reinforce the barotropic component of the low-frequency waves while tending to diminish the baroclinic component of the low-frequency waves. All of these findings give further credence to earlier results for the Northern Hemisphere. As a supplementary to the feedback analyses, the energetics analysis for the winter seasons in both the Northern and the Southern Hemispheres reveals that the forcing of the low-frequency flow by the high-frequency transients in the Southern Hemisphere is much stronger than in the Northern Hemisphere. The contribution of the stationary waves to maintenance of the low-frequency flow through barotropic instability is significantly less in the Southern Hemisphere.

1. Introduction

Despite intense research in recent years, a definitive understanding of the relationship between transients of different scales remains an elusive problem which adversely affects our ability to accurately forecast weather in the extended ranges. Significant advances have been made in our understanding of the relationship between the time-mean circulation and the transient eddies. Hoskins et al. (1983) developed the $\boldsymbol{E}$ vector to relate the shape and propagation of eddies to the feedback of these eddies onto the time mean flow. Simmons et al. (1983) used a barotropic model to conclude that of the different forcing mechanisms which may exist, barotropic instability of the climatological mean wavy state is responsible for the bulk of the observed low-frequency variability. The forcing mechanism of the stationary flow by both low- and high-frequency transients was investigated by Lau and Holopainen (1984). Their results indicate that while the high-frequency eddies act to maintain the barotropic component of the stationary waves, the low-frequency waves tend to diminish the stationary waves (the later is quite consistent with the findings of Simmons et al.).

Cai and Mak (1990), using a two-layer quasi-geostrophic channel model, demonstrated the existence of a symbiotic relationship between high-frequency synoptic scale transients and the low-frequency planetary scale waves. The low-frequency planetary waves gain energy barotropically from the transient eddies. These internally generated low-frequency waves in turn create baroclinically favorable regions for the development of high-frequency transients, forming traveling storm tracks that move together with the planetary scale traveling waves. Robinson (1991a) showed, using a two-level global model, that the vorticity flux associated with synoptic scale waves reinforces the low-frequency eddies while slowing their propagation.

In a two-part study of the Northern Hemisphere

* Corresponding author.

(NH) winter circulation, Cai and van den Dool (1991, 1992; hereafter referred to as CD1 and CD2) documented the existence of traveling storm tracks in the observations and related them to their associated traveling low-frequency waves using a so-called phase-shifting method. The authors showed that the relationship between the low-frequency flow and the traveling storm tracks was analogous to that between the climatological mean waves and the "stationary" storm tracks. The high-frequency transients, organized by the low-frequency waves, act to maintain the barotropic component of the low-frequency flow while weakening the baroclinic component of the large-scale flow.

Several studies focusing on month-to-month variability in the Southern Hemisphere (SH) have recently appeared. Mo and White (1985) and Kidson (1988) showed that changes in the zonally symmetric flow are significant contributors to the observed monthly anomalies (about 25%). Karoly (1990) further argued that the symbiotic relation between high- and low-frequency transients plays an important role in maintaining the zonal component of the low-frequency variation. The modeling studies by Robinson (1991b) and Yu and Hartmann (1993) support the importance of the feedback of high-frequency transients for maintaining the low-frequency variations of the zonally symmetric circulation.

In this paper we extend the work presented in CD1 and CD2 to investigate the roles played by the transient eddies of different scales in maintaining the winter mean SH circulation. Our emphasis lies on the zonally asymmetric component of the low-frequency variation on time scales from a week to a season (i.e., the intraseasonal variability). We aim to increase our understanding of the symbiotic relationship between high- and low-frequency transients and compare the SH results with those of CD1 and CD2 for the NH. This will be accomplished from several perspectives. A climatology of the 500 mb flow is presented, decomposing the flow into its various temporal and spatial components and relating the transient forcing to the mean flow through the use of geopotential height and temperature tendencies. Next we use the phase-shifting technique to ascertain the existence of the traveling storm tracks in SH winter time circulation. We then present an energetics analysis for the winter circulations in both hemispheres (e.g., DJF for the NH and JJA for the SH) to gain insight into the underlying interactive dynamics among the low- and high-frequency transients and the zonally symmetric and asymmetric parts of the time mean flow.

This paper is organized in the following manner. An overview of the data is provided in the next section. In Section 3, a climatology of the winter season 500 mb SH circulation is presented. The interactive relationship between low- and high-frequency transients is examined in Section 4 in three parts: the effects of the high-frequency transients on the low-frequency flow, the relationship between the traveling storm tracks and low-frequency waves, and the energetics of the winter mean circulation in both hemispheres. The results of this study are summarized in Section 5.

2. Data and analysis procedures

The primary database used in this study consists of the twice-daily 500 mb geopotential heights and temperatures from grid-point analyses produced by the European Center for Medium Range Weather Forecasting (ECMWF) for 9 Southern Hemisphere winters (1980–1988), taken to extend from 21 May through 7 September, for a total of (9×220) 1980 analyses. The data are stored in a $2^\circ \times 2.5^\circ$ latitude-longitude grid extending from the equator to the South Pole, resulting in 144 grid points in the zonal direction and 46 grid points in the meridional direction. The quality and accuracy of the ECMWF data set for this period was thoroughly evaluated by Trenberth and Olson (1988) and updated by Trenberth (1992). Prior to 1986 analysis errors adversely affected the divergent wind field and the associated vertical velocity, most notably in the tropics. We utilize the 500 mb geopotential height and temperature fields to derive u, v, and ω in the quasi-geostrophic framework for the SH energetics calculations instead of those analyzed by ECMWF. We believe that this procedure minimizes the inconsistency of the vertical motion field with other fields of the ECMWF analyses during this period. Because our primary diagnostic efforts utilize only the 500 mb geopotential height and temperature fields, the analysis errors in the divergent wind field would have minimum impact on the results of this study.

The energetics calculations for the NH are based on an ECMWF data set consisting of twice-daily analyzed u, v, ω, and T at 500 mb for 6 winter seasons from 1985/86 through 1990/91. Each winter season is defined to last 150 days commencing on 15 October. The data are stored in 2.5° by 2.5° latitude-longitude grids covering the whole hemisphere. This data set has been used in Cai and van den Dool (1994). Because of the improvement of the quality of the divergence field in the ECMWF analyses after 1986, we feel that there is less need to derive the vertical velocity in the quasi-geostrophic framework for the NH energetics calculations.

To separate the high-frequency transients, the low-frequency eddies, and the seasonal mean flow from the total 500 mb height and temperature fields, a temporal Fourier decomposition is used. As in CD1 and CD2, the low-frequency flow (Z^{L} and T^{L}) is defined as that portion of the fields consisting of fluctuations with periods between one week and a season, with the high-frequency transient flow (Z^{H} and T^{H}) consisting of disturbances with periods of less than one week. The time-mean fields ($\bar{Z}$ and $\bar{T}$) are taken to be the nine-year average of the zero-frequency component in each winter season. This simple Fourier decomposition technique has been shown to be adequate to separate the fluctuations into low- and high-frequency ranges as far as such broad band resolution is concerned (CD1 and CD2).

Another set of derived quantities analyzed in this study is the wavy fields of the height and temperature tendency, $\chi^Z(\lambda, \phi, t)$ and $\chi^T(\lambda, \phi, t)$, which are calculated as:

$$\chi^Z(\lambda, \phi, t) = \left\{\nabla^{-2}\left[-\frac{f_0}{g}\nabla\cdot(\boldsymbol{v}'\zeta')\right]\right\}^*, \quad (1)$$

$$\chi^T(\lambda, \phi, t) = \{-\nabla\cdot(\boldsymbol{v}'T')\}^*, \quad (2)$$

where $\boldsymbol{v}'$, ζ', and T' are the transient parts of the geostrophic wind, relative vorticity, and temperature with the desired frequencies (i.e., low- or high-frequency transients), f_0 is the Coriolis parameter evaluated at 45° S latitude, and g is the gravity parameter. The superscript "*" denotes the wavy portion of the corresponding field, calculated by removing the zonal mean at each grid point.

Eqs. (1) and (2) are solved using spectral methods in the global spherical domain with a symmetric expansion of Z and T into the NH. These calculated $\chi^Z(\lambda, \phi, t)$ and $\chi^T(\lambda, \phi, t)$ fields are also subjected to the time filter, producing time-mean, low-frequency, and high-frequency components. The time mean of $\chi^Z(\lambda, \phi, t)$ and $\chi^T(\lambda, \phi, t)$ calculated with high-frequency transients correspond to the barotropic and baroclinic feedbacks of high-frequency transients to the stationary waves (Lau and Holopainen, 1984). The low-frequency components of $\chi^Z(\lambda, \phi, t)$ and $\chi^T(\lambda, \phi, t)$ calculated with high-frequency transients are interpreted as the barotropic and baroclinic feedbacks of high-frequency transients to the low-frequency waves (CD1 and CD2).

The data in each of the figures in this paper were truncated to T21 resolution. To provide maximum clarity and detail in the extratropics, all polar stereographic plots show data poleward of 20° in both hemispheres.

3. Winter time, time circulation and transient eddy forcing

The statistics of the SH circulation have not been as extensively analyzed in the literature as have those of the NH, but a number of comprehensive studies have been completed. Some of the earlier works included those of van Loon (1965), Taljaard et al. (1969), Newton (1972), and Hartmann (1977). The inclusion of satellite data into the analyses has greatly augmented the data sets, leading to a tremendous improvement in the quality and accuracy of SH climatology. Although far from being an inclusive reference list, studies conducted by Trenberth (1979, 1980a, 1980b, 1981, 1991), Trenberth and Mo (1985), Mo and White (1985), Kidson (1988, 1990), Hansen and Sutera (1991), Berbery et al. (1992), and others have provided a sound platform from which to launch additional SH diagnostic studies. The purpose of this section is two-fold: to supplement the available literature regarding the winter-time circulation in the SH, and to provide a reference from which to further examine the relationship between low- and high-frequency transients in the SH.

Shown in Fig. 1 are the winter mean 500 mb geopotential height field and the root-mean-square (rms) fields of both the high- and low-frequency transients. The familiar SH winter-mean 500 mb map, Fig. 1a, indicates a weak dominance of planetary wave number 1 mixed with wavenumber

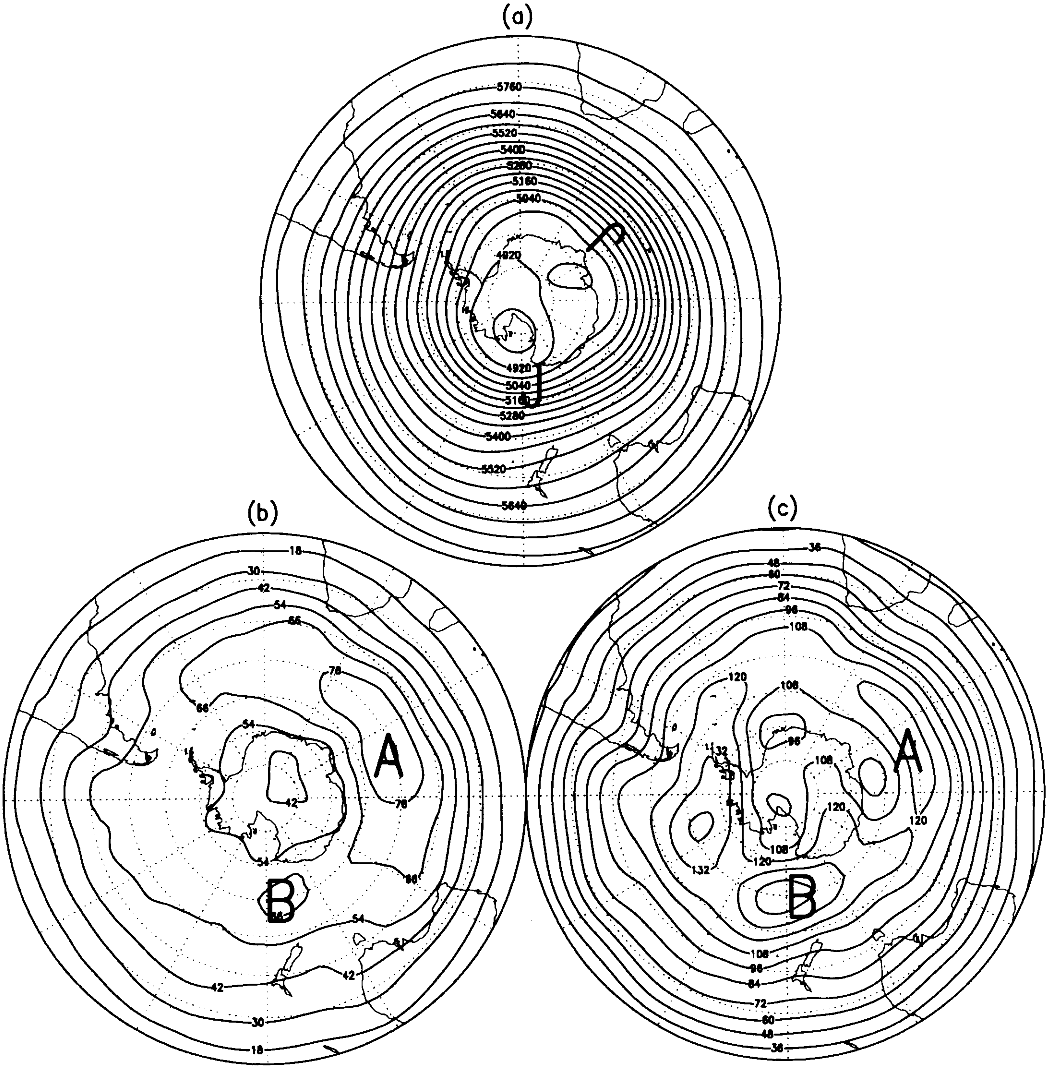

Fig. 1. Statistics of the 500 mb geopotential height field over 9 winter seasons. (a) Time-mean circulation. (b) Standard deviation of the high-frequency transients. (c) Standard deviation of the low-frequency transients. Contour interval for (a), (b) and (c) is 60, 12 and 12 m, respectively.

3 in the polar regions, with mid-latitude troughs evident along longitudes 15° E, 90° E, and 160° W (Van Loon et al. (1993) noticed some evidence of variability of mean circulation in SH at decadal scales, particularly in the zonal wavenumber 3 of the stationary wave field). Due to the geographical differences between the two hemispheres, these troughs are considerably less intense in the SH than are the troughs in the NH. Trenberth (1991) used 300 mb winds to identify two distinct jets: a winter-time sub-tropical jet centered around 30° S and strongest between 100° E and 170° W, and a polar jet which extends between 50° S and 70° S. The two cores of the polar jet are indicated by "J" in Fig. 1a. A distinct split in the winter-mean flow occurs around New Zealand between 140° E and 160° W.

The winter mean storm tracks are seen in the rms field of the high-frequency eddies (Fig. 1b). Unlike the NH, a belt of extensive high-frequency eddy activity nearly circumnavigates the earth between 40° S and 60° S with somewhat zonal asymmetry, being strongest in the Indian Ocean and weakest southeast of South America. The minimum values of the field in the mid-latitudes are nearly 60 m, compared to about 40 m in the NH (CD1). However, maximum values in both hemispheres are quite similar. The maxima of rms field of high-frequency eddies in the southern Indian Ocean (indicated by "A") and south of New Zealand ("B") correspond with the July mean storm tracks identified by Trenberth (1991). Berbery et al. (1992) used teleconnectivity maps to document two wave trains originating near "A" in the southern Indian Ocean and splitting the flow around New Zealand. These two maximum centers of high-frequency variability are located over the equatorward periphery of the two polar jet cores.

The rms map of the low-frequency transients (Fig. 1c) shows locations of maximum values very near to but slightly downstream of those in the high-frequency field (marked again, for reference, as "A" and "B"). The local maximum over the southern Indian Ocean roughly overlaps with the strongest maximum in the high-frequency field ("A"). The greatest low-frequency variability in the winter occurs along 60° S south of New Zealand ("B"), an area found by Trenberth and Mo (1985) to be climatologically favorable for long-term blocking events.

A comparison between the hemispheres of the zonally averaged rms values of the low- and high-frequency transients, Fig. 2, reveals that high-frequency transients are stronger in the SH than in the NH. The amplitude of the low-frequency variability in the SH is 10 to 20% less than in the NH; nevertheless, the low-frequency variability is about 2 times stronger than the high-frequency variability in both hemispheres. The zonally averaged low-frequency variability peaks at 58° S, nearly the same latitude as the high-frequency variability. This is in contrast to the NH, where the maximum of the zonally averaged low-frequency variability occurs at 62° N, well north of the maximum latitude of the high-frequency variability (50° N). It is also of interest to point out that the amplitude of the total transients in the two hemispheres is nearly identical except over the polar regions where the variability of the transients is stronger in the NH (not shown).

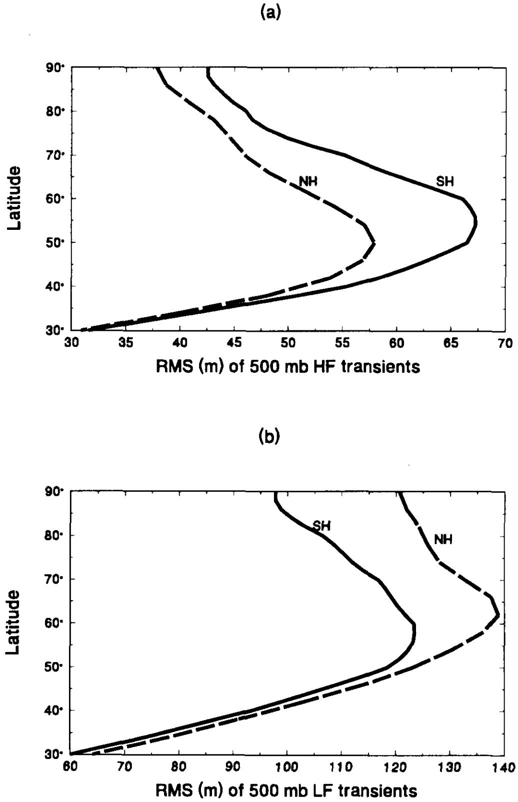

Fig. 2. Zonal mean root-mean-square (rms) of the 500 mb transients as a function of latitude, in meters. (a) High-frequency transients. (b) Low-frequency transients.

We also calculated separately the amplitudes of the zonally symmetric and asymmetric parts of the low-frequency flow. The results indicate that the low-frequency variability in the middle latitudes of both hemispheres is primarily zonally asymmetric in nature (not shown). The zonally symmetric component accounts for less than 10% of the total intraseasonal low-frequency variance in the SH, and somewhat less than 10 to 15% in the NH. Mo and White (1985), Kidson (1988), and Karoly (1990) found that the zonal component of the monthly and interseasonal variability has a larger contribution to the total variance of the monthly or longer fluctuations (up to 25%). Karoly (1990) noticed that the zonally symmetric part of the 5–30 days anomalies explains a smaller fraction of the total 5–30 days variance than the zonally

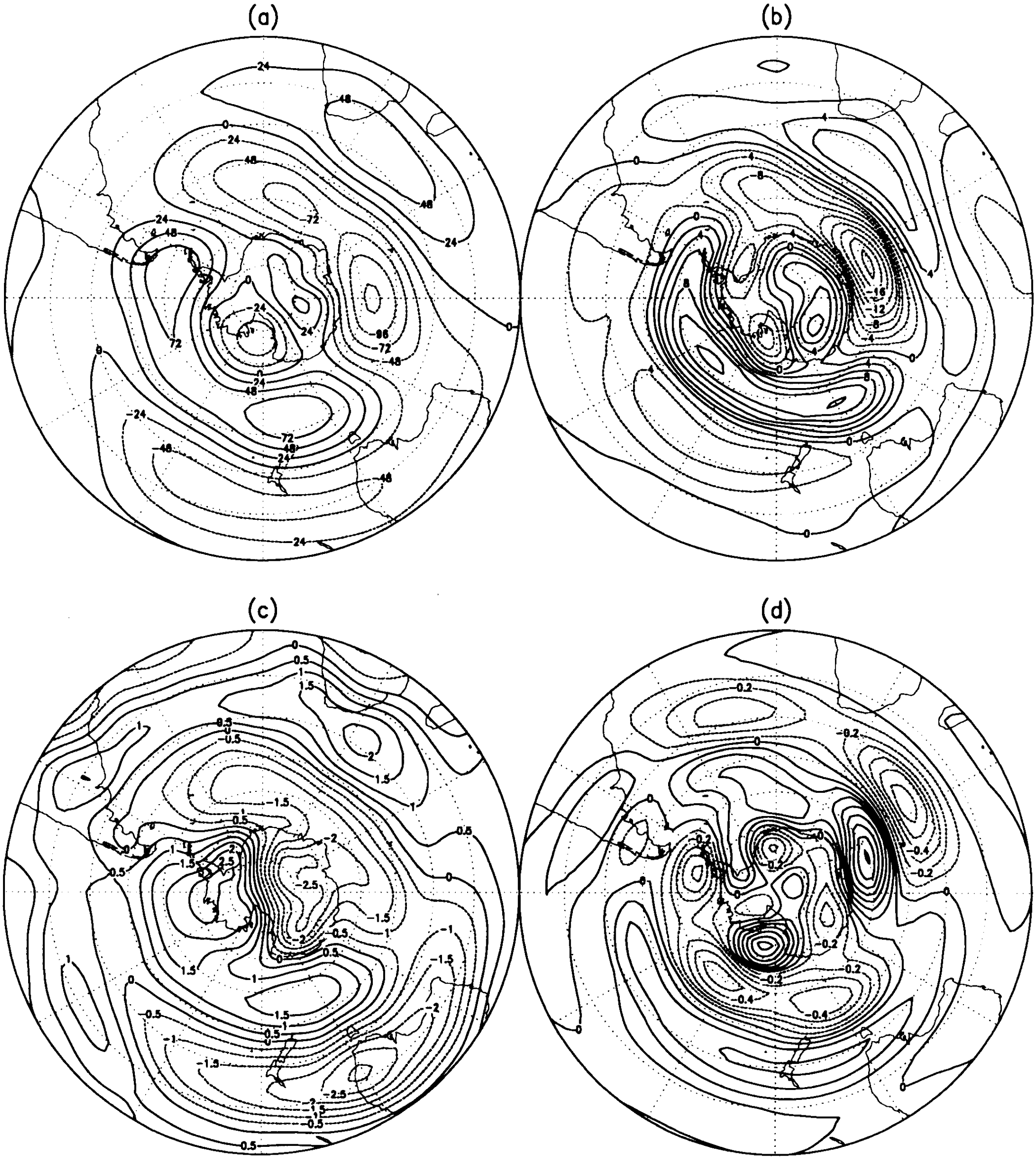

Fig. 3. (a) Total wave field of the winter mean 500 mb geopotential height. (b) Time-mean geopotential height tendency field induced by the high-frequency transients. (c) As in (a), except for the 500 mb temperature field. (d) As in (c), except for the temperature tendency. Contour interval for (a), (b), (c) and (d) is 24 m, 2×10^{-5} m s^{-1}, 0.5°C, and 0.1×10^{-5} °C s^{-1}, respectively.

symmetric part of the fluctuations on monthly or longer scales, which is in fair agreement with our findings.

Now, let us turn our attention to the forcing mechanism of transient eddies on the stationary waves. The winter-mean stationary wave patterns and the height and temperature tendency fields associated with high-frequency eddies are presented in Fig. 3. It is seen that the zonal waves 1 and 3 are strongly evident in the stationary wave fields of both height and temperature (Figs. 3a and 3c). The barotropic feedback of the high-frequency eddies (Fig. 3b) shows a nearly in-phase relationship with the stationary wave field. In the mid-latitude band from 30° to 70° S the pattern correlation between the two maps is 0.73. The baroclinic feedback induced by these eddies (Fig. 3d) is generally out-of-phase with the temperature wave field, with a pattern correlation between these two fields of −0.67 in the mid-latitudes. These results reveal that the forcing mechanism of the high-frequency transients onto the stationary waves in the SH is similar to what has been documented for the NH (Lau and Holopainen, 1984, CD1 and CD2): the vorticity flux associated with the high-frequency transients acts to reinforce the barotropic component of the stationary waves, while the heat flux associated with high-frequency transients acts to diminish the baroclinic part of the stationary waves.

Since the relation between the stationary wave field and the feedbacks of the high-frequency eddies is similar in both hemispheres, it would be legitimate to ask if the same holds true for the relation between the feedbacks of the low-frequency transients and the stationary waves. For the NH, the winter-mean stationary wave field and the height tendency field induced by the low-frequency waves are generally out-of-phase with each other (Fig. 3 in CD1), an indication of barotropic instability of the zonally asymmetric time-mean flow (Simmons et al., 1983). Fig. 4, a counterpart of Fig. 3 in CD1, illustrates the time-mean barotropic feedback of the low-frequency transient waves for the SH. In comparison with the stationary wave field (Fig. 3a), they appear to be in quadrature over the middle and high latitudes (the pattern correlation between the two maps in the areas from 30° to 70° S is −0.25), lending little supportive evidence for the existence of barotropic instability in the SH winter circulation. Further support for this conclusion will be presented in Subsection 4.3.

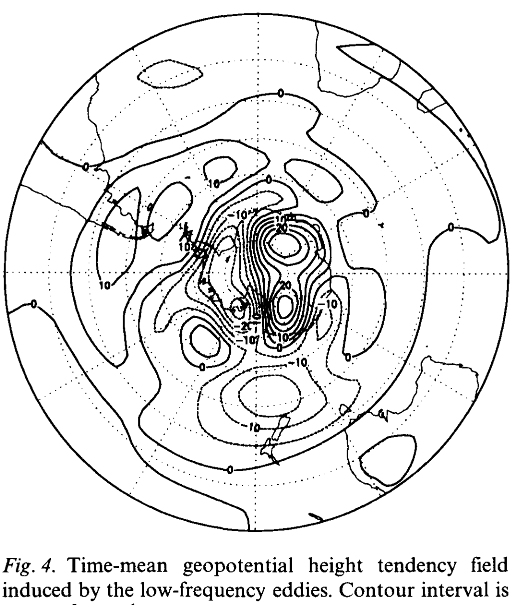

Fig. 4. Time-mean geopotential height tendency field induced by the low-frequency eddies. Contour interval is 5×10^{-5} m s^{-1}.

4. Interactive relationship between low- and high-frequency transients

To attain a global view of the interaction between the low- and high-frequency transients, we present in this section a comprehensive set of statistics for the SH 500 mb mean winter circulation and the energetics of the winter time circulation in both hemispheres. We strive to answer the following questions: Is the forcing mechanism of high-frequency eddies onto low-frequency transients stronger in the SH than in the NH? In CD1 and CD2, the authors argued that the low-frequency transients organize the high-frequency eddies so that the latter could continuously force the former. The key point in this process is the symbiotic relation between low- and high-frequency transients. Is the symbiotic relation also evident in the winter time circulation of the Southern Hemisphere? We also wish to quantitatively compare the contribution to low-frequency variability from the forcing mechanism of high-frequency eddies with that from the instability of climatological winter mean flow in both Northern and Southern Hemispheres. These two are the main known internal forcing mechanisms for low-frequency variability in the Northern Hemisphere.

4.1. Correlation between the high-frequency transient feedback and the low-frequency eddies

The relationship between the low-frequency waves and the high-frequency transients can be inferred by computing the correlation between the low-frequency flow, Z^{L}, and the low-frequency component of the height tendency field induced by the high-frequency eddies, $\{\chi^{Z}_{hf}\}^{L}$. It should be pointed out that unlike a correlation between two arbitrary variables, this correlation should be interpreted as a measure of energy conversion between the low- and high-frequency transients. Specifically, a positive (negative) correlation indicates kinetic energy conversion from (to) high-frequency to (from) low-frequency transients. Hence in the discussions below, we will focus more on the sign of the correlation than on the numerical value itself, which is proportional to the energy conversion rate between low- and high-frequency transients.

Shown in Fig. 5 is the zonally averaged correlation between Z^{L} and $\{\chi^{Z}_{\mathrm{hf}}\}^{\mathrm{L}}$ for both hemispheres. The positive correlation clearly indicates that the vorticity fluxes of high-frequency eddies act as an energy source for low-frequency transients in both hemispheres. It is seen that throughout the mid-latitudes, the correlation in the SH is nearly twice as large as that of the NH. This strongly suggests that the forcing of the mid-latitude low-frequency variability by the high-frequency eddies is significantly more effective in the SH than in the NH. We will come back to this conclusion with more quantitatively supportive results in Subsection 4.3.

The correlation coefficients between the zonally symmetric portion of Z^{L} and $\{\chi^{Z}_{\mathrm{hf}}\}^{\mathrm{L}}$ have also been calculated, but for brevity the plots have been omitted. In both hemispheres, the correlation coefficients exhibit a similar dependency on latitude as in the total fields presented in Fig. 5. This implies that the rates of energy conversion from the high- to low-frequency transients for both the zonally symmetric and asymmetric components are quite comparable.

The geographical distributions of the correlation between Z^{L} and $\{\chi^{Z}_{\mathrm{hf}}\}^{\mathrm{L}}$ for both hemispheres are

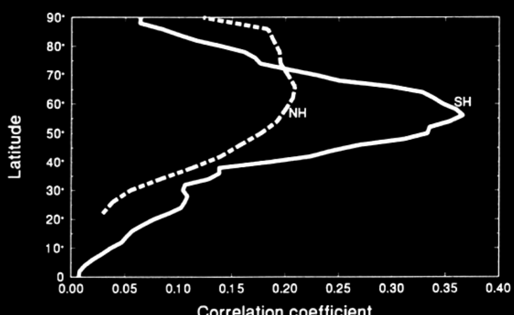

Fig. 5. Zonal mean of the correlation of the low-frequency transients in the 500 mb height field and the low-frequency component of the height tendency induced by the 500 mb high-frequency transients for both hemispheres as a function of latitude.

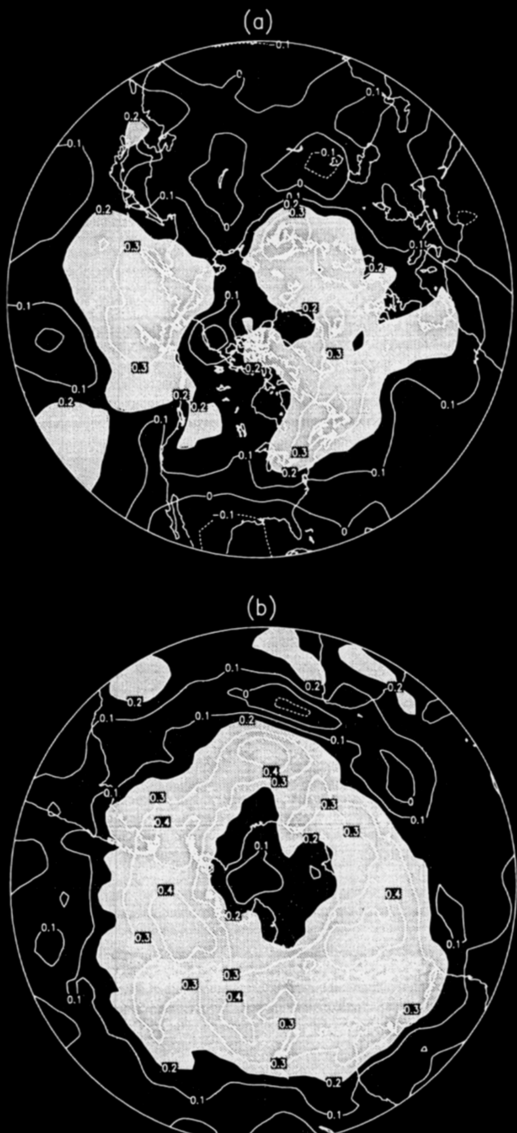

Fig. 6. Time-mean correlation of the low-frequency eddies in the 500 mb height field with the low-frequency component of the height tendency induced by the 500 mb high-frequency transients for (a) the Northern Hemisphere and (b) the Southern Hemisphere. Contour interval is 0.1, with values greater than 0.2 shaded.

illustrated in Fig. 6. The major difference between the two maps is the stronger zonal asymmetry on the NH map (Fig. 6a) and the nearly zonally uniform kinetic energy conversion from the high- to low-frequency transients for the SH in the latitude belt from 30° S to 60° S (Fig. 6b). Recall that there also exists a stronger zonal symmetry (asymmetry) in the rms field of the low-frequency transients in the SH (NH). Such a coincidence between patterns of low-frequency variability and the patterns of the forcing of high-frequency eddies in both hemispheres is quite suggestive of the conclusion that the forcing of high-frequency eddies is a main player in generating low-frequency variability in both hemispheres.

4.2. Existence of traveling storm tracks

In CD1, the authors presented a method of special composite analysis (phase-shifting method) designed to identify the time-mean structure of the low-frequency waves and their attendant traveling storm tracks. As in a geographically fixed coordinate system, the phase-shifting technique enables us to construct various statistics of the transients in a moving frame that has a speed equal to the instantaneous phase speed of an individual low-frequency wave of a reference variable (say Z^{L}) at a reference latitude ϕ_0. Using this transformation, the traveling wave and its attendant features become fixed in space, separated from the remainder of the flow. Taking an ensemble mean (or time mean) of the reference variable in this moving frame (several winter seasons, at least) yields the mean structure of the low-frequency wave being followed. The ensemble mean of the high-frequency variability calculated in the same moving frame would give us a hint of the existence of traveling storm tracks associated with that low-frequency wave. Similarly, the ensemble mean of other variables in the same moving frame enables us to examine the relationship between the low-frequency wave and the patterns of the other variables. Particularly, we would like to examine the spatially coherent relationship between the low-frequency waves and the feedback fields of the high-frequency eddies. Readers are referred to Appendix A for more details of the phase-shifting method.

As in CD1 and CD2, the low-frequency wave with zonal wavenumber equal to either 1, 2, 3, and 4 of the 500 mb geopotential height is used in this study to construct the moving frames. The reference latitude is selected to be 56° S as it is the latitude where the maximum variability in both the low- and high-frequency transients occurs (Fig. 2). Calculations using various reference latitudes between 40° S and 60° S (not presented) indicate that the general characteristics of the statistics calculated in the moving frames are not particularly sensitive to the choice of the reference latitude. The success of using the phase-shifting method to diagnose the symbiotic relation between high- and low-frequency transients lies in its ability to separate the traveling storm tracks from the stationary ones. In CD1, the authors argued that if the moving frame produces little preference over any longitudinal sectors, the signal of stationary storm tracks is effectively removed from the rms field of the high-frequency eddies calculated in a moving frame. As seen in Appendix A, a histogram analysis (Fig. 12), prepared in the same manner as Fig. 10 in CD1, reveals that the four moving frames used in this study do not show statistically significant preference over any longitude sectors. Therefore, any zonal inhomogeneity appearing in the rms map of the high-frequency eddies calculated in a moving frame would correspond to the traveling storm track associated with the low-frequency wave being followed.

Each of the Figs. 7–10 contains 4 maps illustrating the statistics of 6 variables calculated in one moving frame with $m = 1$ for Fig. 7, $m = 2$ for Fig. 8, $m = 3$ for Fig. 9, and $m = 4$ for Fig. 10. All 4 figures are prepared in the same fashion. Land masses are excluded as they have no relevance on the mean maps in the moving frames. Panel (a) of the figures shows two parameters: the time-mean height field of the low-frequency transients, contoured every 12 m, and the associated traveling storm tracks, shaded and superimposed. The traveling storm tracks are defined as the regions of maximum high-frequency eddy activity in terms of their rms values calculated in the moving frames. Based on the simple model study by Cai and Mak (1990) and the observational evidence presented in CD1 and CD2 for the NH, one would expect traveling storm tracks to exist in the region of the anomalous westerly wind. As seen in panel (a) of Figs. 7 through 10, the most significant storm tracks are over the trough regions, while less extensive storm tracks can be found in the anomalous westerly wind around the poleward periphery of

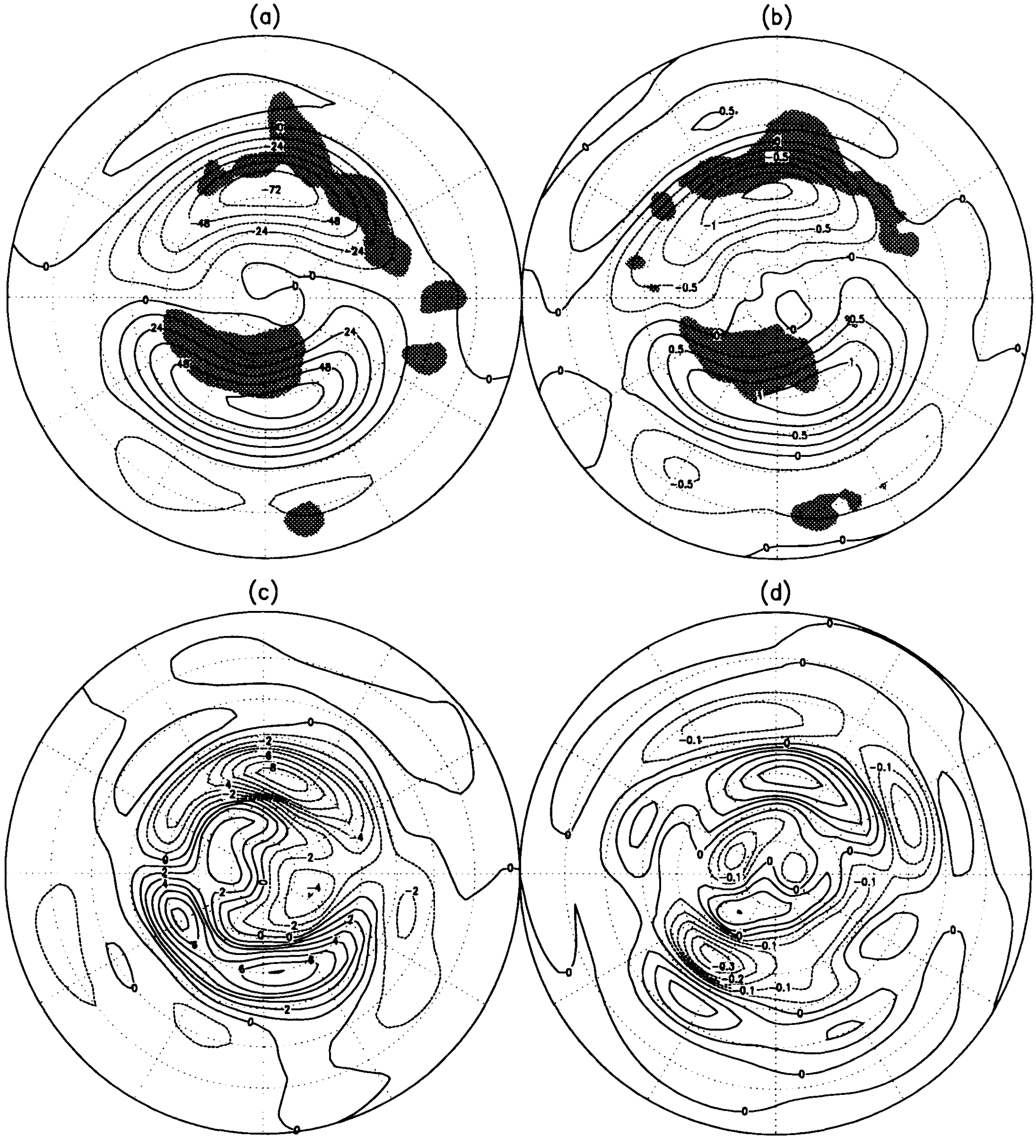

Fig. 7. Statistics of the winter mean 500 mb circulation in the moving frame with $m = 1$. (a) Time-mean geopotential height of low-frequency transients, contour interval is 12.0 m; shaded regions represent the traveling storm tracks, where the departure from the zonal mean of the standard deviation of the high-frequency eddies exceeds 2.0 m. (b) As in (a) except for the temperature field, contour interval is 0.25°C; (c) Time-mean height tendency field induced by the high-frequency eddies, contour interval is 1.0×10^{-5} m s^{-1}. (d) as in (c), but for the temperature tendency, contour interval is 0.05×10^{-5} °C s^{-1}.

the ridges. This pattern is most striking for wave numbers 3 and 4 (Figs. 9a and 10a).

Panel (b) in the 4 figures is identical to panel (a) except that temperature data are used. The temperature fields are contoured in 0.25°C increments. The ensemble mean temperature fields calculated in the moving frames generally lag the corresponding height fields westward by about 10° but otherwise display an identical pattern. The shaded portions of panel (b) illustrate the traveling storm

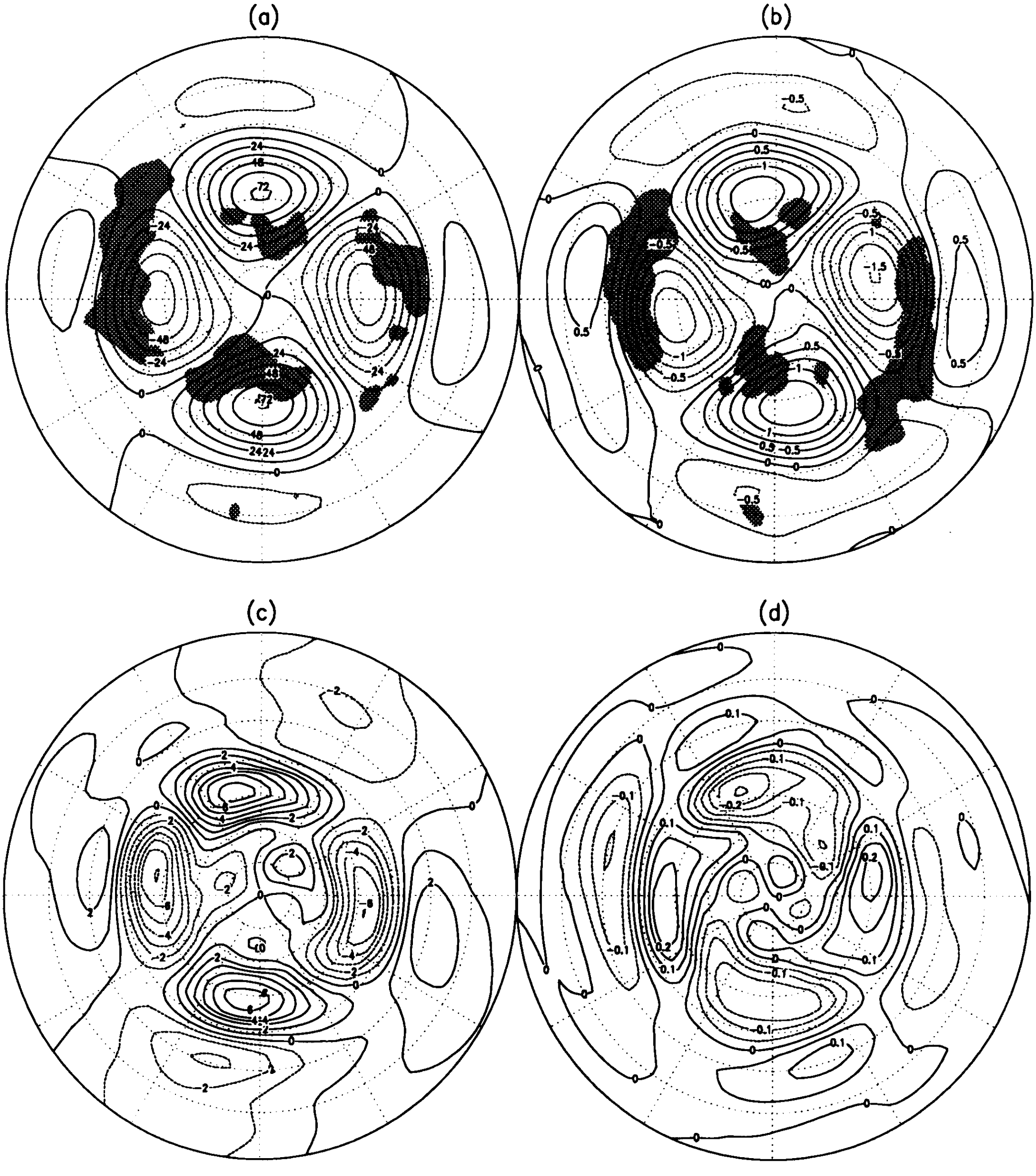

Fig. 8. As in Fig. 7, except for $m = 2$.

track in the temperature field, defined as zonal maxima of the rms of the high-frequency temperature transients in the same moving frame as that in panel (a). The traveling storm tracks in the temperature field are evident in generally the same areas as their counterparts in the height field, downstream and equatorward of the low-frequency troughs and, to a lesser extent, downstream and poleward of the ridges.

The barotropic feedback of the high-frequency eddies onto the low-frequency waves is obtained by computing the ensemble mean of the geopotential height tendencies associated with the high-frequency transients in the moving frames. These

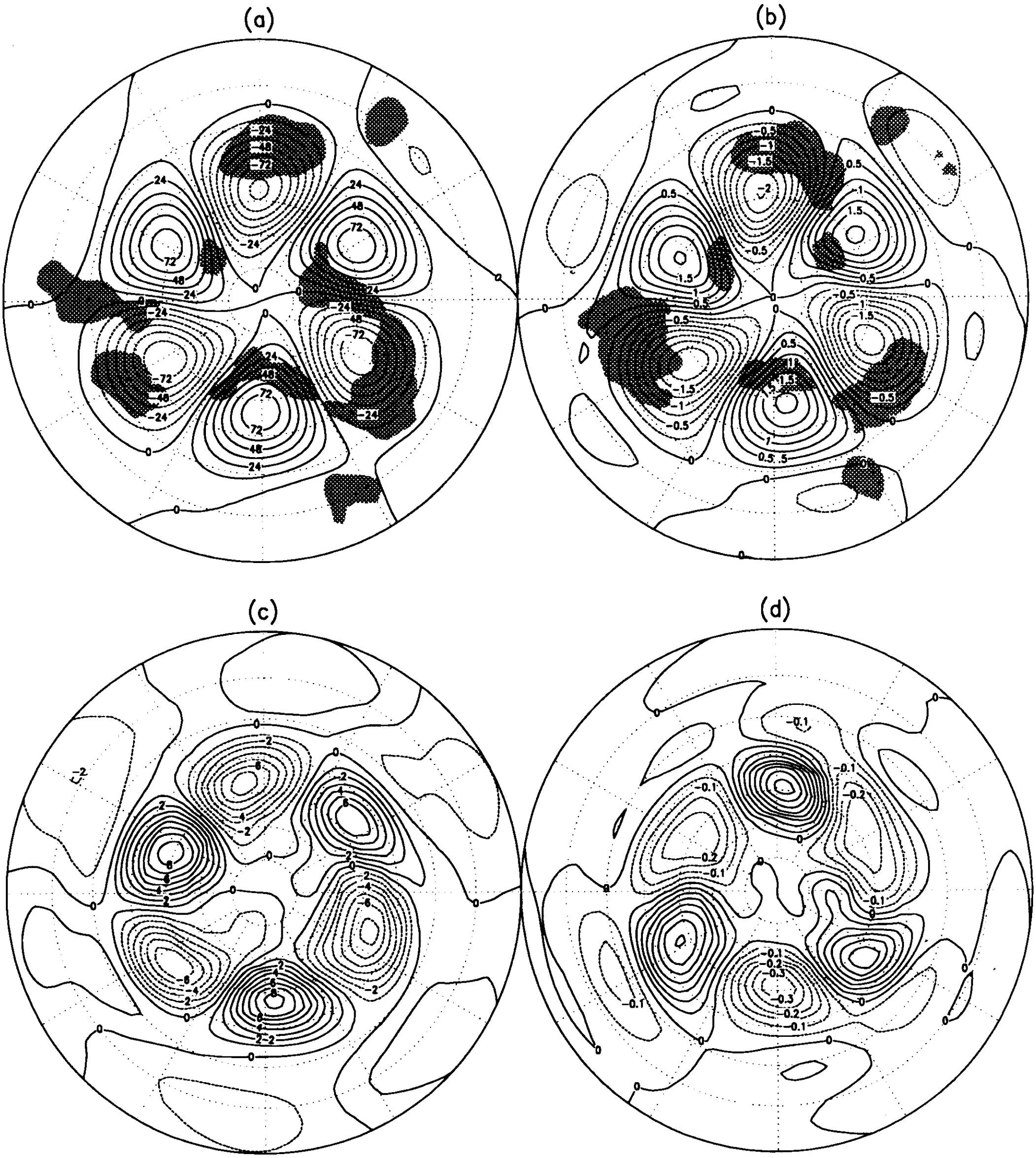

Fig. 9. As in Fig. 7, except for $m = 3$.

results are presented in panel (c) of Figs. 7 through 10. The tendency fields capture most of the features shown in the corresponding low-frequency fields. This nearly in-phase relationship between panels (a) and (c) in Figs. 7 through 10 clearly illustrate the constructive barotropic feedback of the traveling storm tracks onto the low-frequency waves, as the geopotential height tendencies act to intensify the height field.

Panel (d) of Figs. 7 through 10 displays the ensemble mean baroclinic feedback of the high-frequency transients onto the low-frequency transients. These tendency fields correlate very well with the maps shown in panel (b) except the

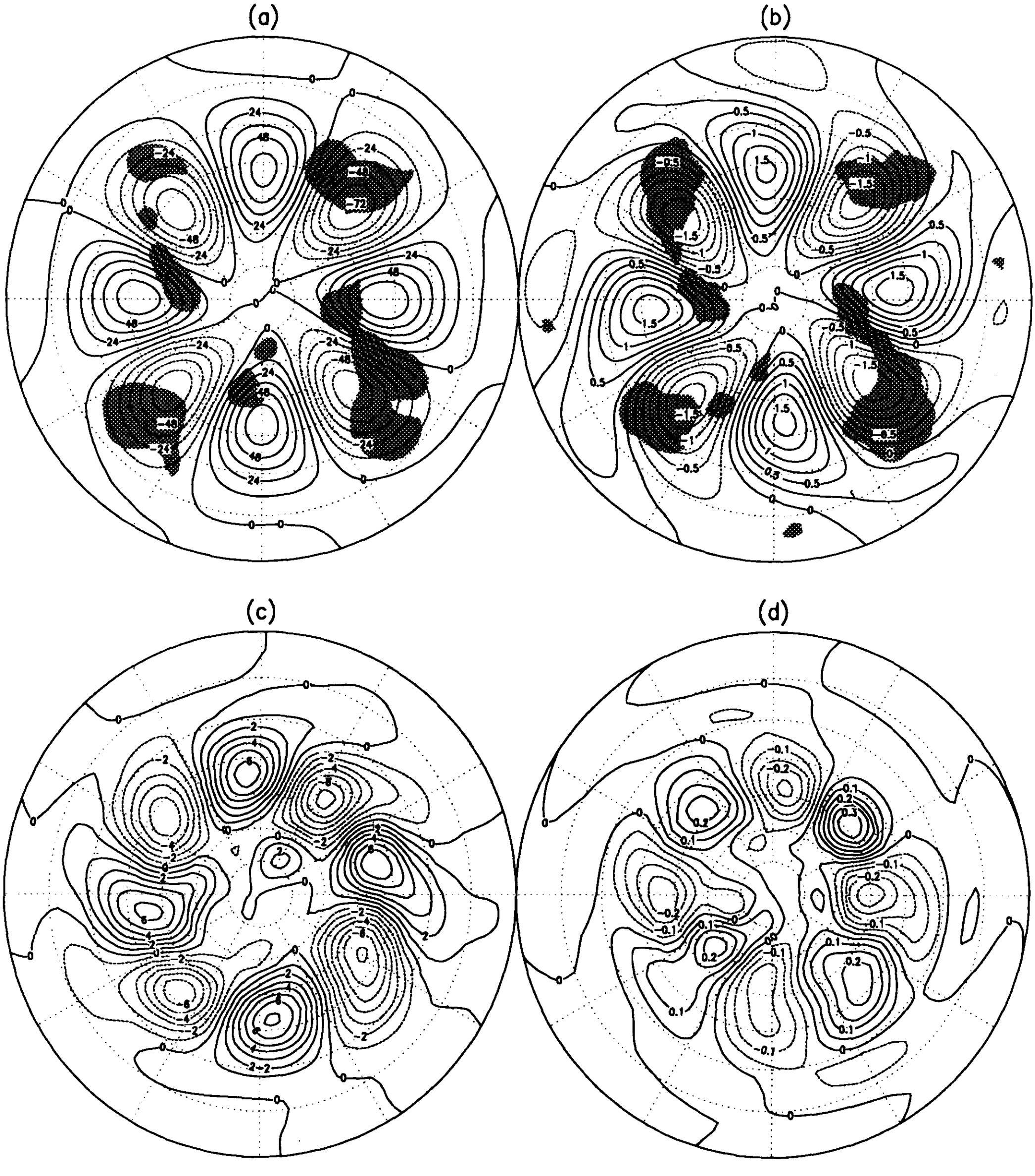

Fig. 10. As in Fig. 7, except for $m = 4$.

difference in sign, showing an out-of-phase relationship. This indicates that the heat flux associated with the high-frequency eddies acts to damp the baroclinic component of the low-frequency waves, hence weakening the low-frequency waves in the absence of the barotropic feedback.

Fig. 11 provides a synopsis of these findings. Displayed for zonal wave number 1 through 4 are the map correlations between panels (a) and (c), a measure of barotropic feedback, and between panels (b) and (d), indicative of baroclinic feedback, in the mid-latitude band of 30°–70° S for Figs. 7 through 10 (or for the zonal wavenumber 1 through 4). The pattern correlations between

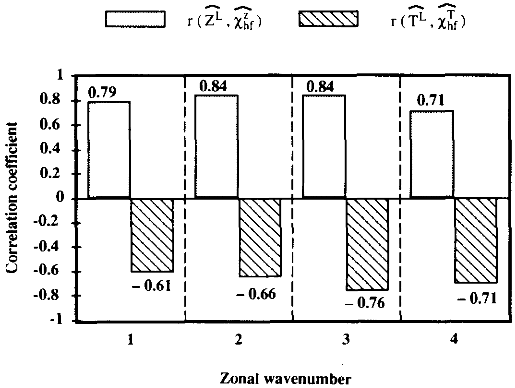

Fig. 11. Pattern correlations for maps displayed in Figs. 7 through 10 in the mid-latitude band from 30° to 70°S. For each zonal wavenumber, the shaded bar is the correlation coefficient between panels (a) and (c) and the hatched bar the correlaction coefficient between panels (b) and (d). Values of the correlation coefficient are indicated above each bar.

panel (a) and (c) are in the range from 0.78 to 0.84, and for panels (b) and (d) are in the range from −0.76 to −0.61, indicating the homogeneity of the results presented above with respect to the zonal wavenumber.

In addition to a well-defined zonal structure, the low-frequency waves have a distinct meridional structure. For all four waves, meridional wave number 2 is strongly evident. Polarity reverses in the height and temperature fields at about 30° S for $m = 4$, around 35° S for $m = 3$, and near 40° S for $m = 2$. A tripolar structure is noted in both hemispheres for $m = 1$, with polarity reversals occurring at about 80° S as well as 40° S. Of course, the exact latitudes of the nodal shown on the maps presented in Figs. 7 through 10 move with the reference latitude for constructing the moving frames.

In summary, Figs. 7 through 11 illustrate the existence of traveling storm tracks in the SH similar to those reported in CD1 and CD2 for the winter time circulation of the NH. These storm tracks develop preferentially in trough regions of their attendant traveling low-frequency waves where the anomalous wind is westerly. The positive correlation between the low-frequency flow and the barotropic feedback fields indicates that the vorticity flux induced by the high-frequency eddies acts to maintain the barotropic component of the low-frequency waves, and this feedback in the SH is about twice the strength of that in the NH. The heat flux induced by the high-frequency eddies, however, weakens the baroclinic portion of the low-frequency flow, as evidenced by the out-of-phase relationship between the baroclinic feedback and the low-frequency temperature fields. The dynamical relationship between the traveling storm tracks and the low-frequency transients is analogous to that for the stationary storm tracks and the stationary waves shown in Figs. 1 and 3.

4.3. *Energetics analysis*

To lend further quantitative support to results obtained with the feedback analyses, we report in this section the results of an energetics analysis for the transients of different scales in both hemispheres. The emphasis is on the comparison of the energetics of the winter circulation for the two hemispheres. A number of energetics studies are available in the literature, some emphasizing scale interactions. Recently, for example, Sheng and Derome (1991) performed energetics analyses for the NH by separating the transients into their low- (slow) and high- (fast) frequency components for the winter and summer seasons. Their results suggest that both the instability of winter time climatological circulation and the forcing of high-frequency eddies act as energy sources for the low-frequency variability in the NH.

In order to diagnose the relative importance of zonal asymmetry in the time-mean flow and forcing of the transients of different scales in both hemispheres, we have taken another approach in viewing the wintertime energetics. In addition to separating the transient flow into its low- and high-frequency temporal components, we have further partitioned the time-mean flow into its symmetric and asymmetric portions. The winter time-mean and globally averaged energetics at 500 mb could be viewed as an approximation to the vertically and globally averaged energetics of the winter time mean circulation.

It is straightforward to derive the energetics equations for both low- and high-frequency transients. For brevity, we here only present the symbolic form of these equations as follows:

$$
\begin{aligned}
\frac{\mathrm{d}}{\mathrm{d}t}(P^{\mathrm{L}}) &= C(\mathrm{ZON}, P^{\mathrm{L}}) + C(\mathrm{STN}, P^{\mathrm{L}}) \\
&\quad - C(P^{\mathrm{L}}, K^{\mathrm{L}}) - C(P^{\mathrm{L}}, P^{\mathrm{H}}) + G(P^{\mathrm{L}}), \\
\frac{\mathrm{d}}{\mathrm{d}t}(P^{\mathrm{H}}) &= C(\mathrm{ZON}, P^{\mathrm{H}}) + C(\mathrm{STN}, P^{\mathrm{H}}) \\
&\quad - C(P^{\mathrm{H}}, K^{\mathrm{H}}) + C(P^{\mathrm{L}}, P^{\mathrm{H}}) + G(P^{\mathrm{H}}), \\
\frac{\mathrm{d}}{\mathrm{d}t}(K^{\mathrm{L}}) &= C(\mathrm{ZON}, K^{\mathrm{L}}) + C(\mathrm{STN}, K^{\mathrm{L}}) \\
&\quad + C(P^{\mathrm{L}}, K^{\mathrm{L}}) + C(K^{\mathrm{H}}, K^{\mathrm{L}}) - D(K^{\mathrm{L}}), \\
\frac{\mathrm{d}}{\mathrm{d}t}(K^{\mathrm{H}}) &= C(\mathrm{ZON}, K^{\mathrm{H}}) + C(\mathrm{STN}, K^{\mathrm{H}}) \\
&\quad + C(P^{\mathrm{H}}, K^{\mathrm{H}}) - C(K^{\mathrm{H}}, K^{\mathrm{L}}) - D(K^{\mathrm{H}}).
\end{aligned}
\tag{3}
$$

The readers may consult Sheng and Derome (1991) for most of the details in deriving the equations of energetics (as mentioned earlier, we here have taken an extra step of partitioning the time-mean flow into its symmetric and asymmetric portions).

In (3), the P and K terms indicate reservoirs of available potential and kinetic energy associated with low-frequency (superscript "L") and high-frequency (superscript "H") transients. G terms denote generation of available potential energy, and kinetic energy dissipation is represented by the D terms. The C terms represent energy conversions among the disturbances at different time scales. $C(\mathrm{ZON}, P')$ represents the baroclinic energy conversion from the zonally symmetric part of the winter mean flow to either low- or high-frequency transients, and $C(\mathrm{STN}, P')$ represents the baroclinic energy conversion from the stationary wave portion of the winter mean flow to the transients with desired time scales. The $C(\mathrm{ZON}, K')$ and $C(\mathrm{STN}, K')$ terms represent the barotropic energy conversion from the zonally symmetric and asymmetric mean flow to the transients with desired time scales. Non-linear energy transfers of kinetic and available potential energy between the eddies of different scales are denoted by $C(K^{\mathrm{H}}, K^{\mathrm{L}})$ and $C(P^{\mathrm{L}}, P^{\mathrm{H}})$, respectively. The $C(P', K')$ terms represent a conversion from available potential to kinetic energy of the transients with the same time scales. We may evaluate all the terms on the right-hand side of (3) directly from the data at each observation time except the D and G terms. But the time-mean values of the D and G terms could be determined as residuals in (3) by forcing the time-mean value of the left-hand side of the equations to be zero.

The winter time and hemispherical mean energetics for both hemispheres are presented in Fig. 12. Because of the uncertainties in evaluating

Hemispheric Mean Energetics of the winter–time 500 mb Circulation

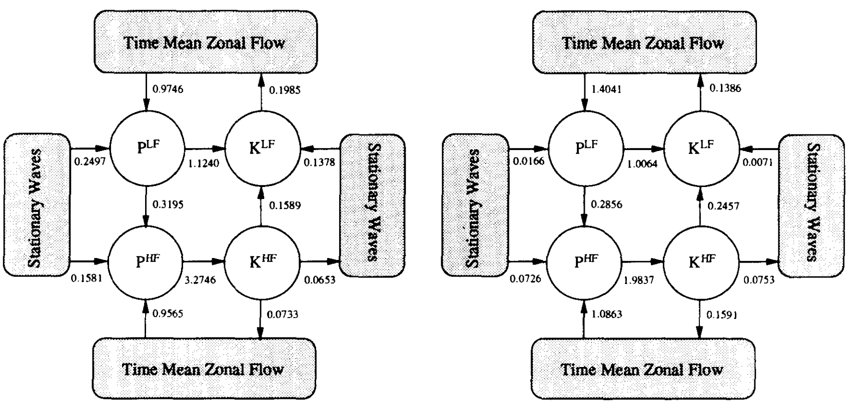

(a) Northern Hemisphere (b) Southern Hemisphere

Fig. 12. The hemispheric mean energetics of the winter time circulation in (a) the Northern Hemisphere and (b) the Southern Hemisphere. Values are in units of W m^{-2}.

each term on the right hand side of eq. (3), we deliberately exclude the G and D terms estimated as residuals in balancing (3). The shaded rectangular boxes indicate the zonally symmetrical (zonal; ZON) and asymmetrical (stationary wave; STN) portions of the time-mean flow, and the circles the reservoirs of the transient eddies. Generally, all of the terms in both hemispheres are of the same sign and order of magnitude. A glaring difference exists between the two hemispheres in the numerical values of two energy conversion terms, namely $C(\mathrm{STN}, P^{\mathrm{L}})$ and $C(\mathrm{STN}, K^{\mathrm{L}})$. The values of $C(\mathrm{STN}, P^{\mathrm{L}})$ and $C(\mathrm{STN}, K^{\mathrm{L}})$, a measure of instability of the zonally asymmetric part of the time-mean flow, for the SH are about two orders of magnitude smaller than those for the NH. This supports the conclusion made by correlating the stationary wave pattern (Fig. 3a) and the time-mean barotropic tendency induced by the low-frequency transients (Fig. 4), which is only about -0.25: in the SH, the instability of the zonally asymmetric part of mean circulation is a nearly insignificant player in generating the mid-latitude low-frequency variability.

A hemispheric comparison of the conversion term $C(K^{\mathrm{H}}, K^{\mathrm{L}})$, which describes the upscale energy cascade to the low-frequency waves from the high-frequency transients (if $C(K^{\mathrm{H}}, K^{\mathrm{L}}) > 0$), yields some very elucidating information. In both hemispheres, it has a positive value, as expected from the correlation calculations presented in Figs. 5–6. But, this term has a value of 0.2457 W m^{-2} in the SH about 50% greater than that in the NH. This is quite consistent with the results shown in Fig. 5 which indicates that the forcing of the low-frequency transients by the high-frequency eddies is significantly stronger in the SH.

It is also important to note that the baroclinic energy conversion from the time mean zonal flow to the low-frequency transients, $C(\mathrm{ZON}, P^{\mathrm{L}})$, in both hemispheres is comparable with that from the time mean zonal flow to the high-frequency transients, $C(\mathrm{ZON}, P^{\mathrm{H}})$. The same is also true for the energy conversion from potential energy to kinetic energy of the low-frequency transients [i.e., $C(P^{\mathrm{L}}, K^{\mathrm{L}})$ versus $C(P^{\mathrm{H}}, K^{\mathrm{H}})$]. These two findings would suggest that classic baroclinic instability also plays an important role in generating low-frequency variability. In light of this, one may argue that part of low-frequency variations could simply be related to the slower phase speeds of the transients rather than to the less (baroclinic) instability of the transients. An on-going study by van den Dool and Cai (personnel communications) on the propagation of the transients in both hemispheres seems to suggest that the transient waves in the SH indeed propagate faster than those in the NH, which offers a kinematic view on the fact the high-frequency (low-frequency) variability in the SH is stronger (weaker) than its counterpart in the NH.

Another issue concerns the net energy conversion between the low- and high-frequency transients. It has been shown that the high-frequency eddies have a positive (negative) barotropic (baroclinic) feedback effect on the low-frequency waves. The feedback calculation seems to agree with energetics calculation shown in Fig. 12 which indicates that the high-frequency eddies deposit (receive) kinetic (potential) energy into (from) the low-frequency waves. Such dual feedback effect of the high-frequency eddies on the low-frequency waves seems to complicate the notion of the forcing mechanism of low-frequency waves by high-frequency eddies. To clarify this issue, we have performed a multi-level calculation only for the terms $C(P^{\mathrm{L}}, P^{\mathrm{H}})$ and $C(K^{\mathrm{H}}, K^{\mathrm{L}})$ with the Northern Hemisphere dataset from 1000 mb to 100 mb derived from ECMWF analyses for the same six winter seasons from 1985/86 through 1990/91 as described in Section 2. The barotropic energy conversion from high-frequency eddies to low-frequency waves is strongest at 300 mb and the baroclinic energy conversion from low-frequency waves to high-frequency eddies has a peak value at 850 mb. The vertically integrated energetics reveal that the high-frequency eddies in the mean indeed act as an energy source to the low-frequency waves because the barotropic energy conversion from high-frequency eddies to low-frequency waves (0.2405 W m^{-2}) is larger than the baroclinic energy conversion from low-frequency waves to high-frequency eddies (0.1859 W m^{-2}). Hence our energetics analysis support the notion of the forcing mechanism of low-frequency waves by high-frequency eddies.

5. Concluding remarks

This paper reports a diagnostic study on the interactive relationship between low- and high-frequency transients with 9 years of ECMWF

500 mb wintertime geopotential height and temperature data for the SH, with emphasis on the comparison with the NH counterparts. Our main findings are follows.

(1) The vorticity flux associated with the time-mean high-frequency transients acts to reinforce the barotropic component of the stationary flow, while the associated heat flux acts to diminish the baroclinic component. This supplements the findings previously documented for the NH by Lau and Holopainen (1984), CD1, and CD2.

(2) The barotropic feedback field induced by the low-frequency transients is in quadrature with the stationary wave field in the SH; however, these two fields are nearly out-of-phase with each other in the NH, an indication of barotropic instability in the NH winter time-mean circulation. Therefore, barotropic instability in the time-mean is less evident in the SH than in the NH as a mechanism for generating low-frequency variability. Further evidence of this lies in hemispheric mean energetics calculations, which indicate that instability due to the stationary waves is about 2 orders of magnitude less in the SH than in the NH.

(3) The forcing due to high-frequency transients plays a greater role in generating low-frequency variability in the SH than in the NH, as evidenced by Figs. 5–6. Energetics calculations support this, as the upscale barotropic energy conversion is about 40% higher in the SH than in the NH. This partially explains why the amplitude of low-frequency variability in the SH is as large as the counterpart in the NH even through that there is lack of stationary wave forcing in the SH.

The SH results presented in this paper supplement those of CD1 and CD2 for the NH concerning the relationship between the low-frequency waves and their associated traveling storm tracks and lend further credence to the findings by Cai and Mak (1990), CD1, CD2, and Robinson (1991a) on the symbiotic relationship between the low-frequency waves and high-frequency eddies. The presence of the traveling low-frequency waves alternates the background baroclinicity in which the high-frequency eddies are embedded. The high-frequency eddies tend to develop preferentially in the downstream region of local maximum baroclinicity through local baroclinic instability. The developing high-frequency eddies in turn surrender their kinetic energy to the low-frequency waves via an up-scale energy cascade process. Such positive barotropic feedback is essential for the low-frequency waves to organize continuously the high-frequency eddies. This symbiotic relationship is analogous to that between the stationary waves and the high-frequency eddies.

Throughout this study, as well as in CD1, CD2, and numerous others as cited throughout this paper, low-frequency variability has been linked to the barotropic forcing of the high-frequency transients largely because of its resemblance to the feedback fields. This is clearly evident in Figs. 5–6 as well as in Figs. 7 through 10. However, as presented by Cai and van den Dool (1994), the total tendency in the low-frequency flow is due to many terms. The barotropic feedback of the high-frequency transients onto the low-frequency flow is actually one of the smallest contributors to the total tendency. While the other components of the tendency field are much larger, they tend to contribute primarily to propagation of the low-frequency eddies and show a lot of cancellation. However, the tendency field induced by the high-frequency eddies contributes significantly to the maintenance of the low-frequency flow, and it remains a vital contributor to the dynamics despite its relative smallness. From an energetics point of view, the nearly in-phase relationship between the barotropic feedback induced by the high-frequency transients and the low-frequency waves implies a kinetic energy conversion from the high-frequency transients to the low-frequency waves, a fact that is supported by the energetics analysis presented in Subsection 4.3.

6. Acknowledgments

The authors are grateful for the support and suggestions that Huug M. van den Dool provided throughout this research. Comments made by the editor and two anonymous reviewers led to an improvement in the clarity of this manuscript. Finally, our sincere thanks go to Brian Doty who, at our request, updated the COLA/UMCP Grid Analysis and Display System (GrADS) system to conveniently handle and display data in polar stereographic form, to our specifications. This research was supported by the National Science Foundation, under grant number ATM-9103647.

Part of the computations were performed on the Cray Y-MP supercomputer at National Center for Atmospheric Research.

7. Appendix

Phase shifting method

In CD1, the authors introduced a special composite analysis (so-called "phase-shifting") method designed to identify the time-mean structure of the low-frequency waves and their attendant traveling storm tracks. The phase-shifting technique allows the flow to be viewed in a coordinate system moving at the instantaneous phase speed of a low-frequency wave in a reference variable at a reference latitude. We refer to the flow viewed in the moving frame as the "phase-shifted" flow in distinguishing it from the flow observed in the geographically fixed coordinate system. The traveling wave and its attendant features becomes fixed in space in the moving frame and are separated from the remainder of the flow. Taking an ensemble mean (or time mean) of the reference variable in the moving frame (over several winter seasons, at least) yields the mean structure of the low-frequency wave being followed (e.g., panel (a) of Figs. 7–10). The ensemble mean of the high-frequency variability calculated in the same moving frame enables us to identify the traveling storm tracks associated with that low-frequency wave (e.g., panel (b) of Figs. 7–10). Similarly, the ensemble mean of other variables in the same moving frame enables us to examine the relationship between the low-frequency wave and the patterns of the other variables (for example, panel (c) of Figs. 7–10 displays the feedback fields of the high-frequency eddies recorded in the moving frames).

The phase-shifted flow can be constructed in the following fashion. Let $\hat{\xi}(\lambda, \phi, p, t)$ be the phase-shifted flow to be constructed from the original flow $\xi(\lambda, \phi, p, t)$, where ξ can be geopotential height, temperature or any observed/derived variables. The phase-shifting formula is

$$\hat{\xi}(\lambda, \phi, p, t) = \xi(\lambda - \lambda^*(t; \phi_0, p_0, \text{other reference parameters}), \phi, p, t), \quad \text{(A1)}$$

where $\lambda^*(t;\ \phi_0,\ p_0$, other reference parameters) is a function of time only and measures the phase angle by which the map $\xi(\lambda, \phi, p, t)$ has to be longitudinally shifted at time t to become $\hat{\xi}(\lambda, \phi, p, t)$. In (A1), ϕ_0 and p_0 are the reference latitude and pressure, respectively. The other reference parameters, such as the reference variable, reference pattern, and reference time, also enter the choice of λ^*. The reference variable and pattern together with the reference latitude and pressure determine the target to be followed in the process of transforming the map $\xi(\lambda, \phi, p, t)$ to the map $\hat{\xi}(\lambda, \phi, p, t)$. The reference time gives us a choice of the lagged, simultaneous, or lead phase shifting relative to the target.

In this study, we have chosen four reference patterns in constructing the phase-shifted flow. They are the low-frequency waves of geopotential height with zonal wavenumber $m = 1$, 2, 3, and 4 at the reference latitude $\phi_0 = 56°$ S, the reference pressure level $p_0 = 500$ mb, and at time t (a simultaneous phase shifting). The results have been displayed in Figs. 7 through 10, respectively. Specifically, we use the following equation to determine λ^*:

$$\lambda^*(t) = \frac{360}{2\pi} \frac{Q_m(t) - Q_m^{\text{new}} - 2\pi R_m(t)}{m}, \quad \text{(A2)}$$

where $Q_m(t)$ is the phase angle of the low-frequency wave m of the 500 mb geopotential height at latitude 56° S at time t, and Q_m^{new} specifies the new longitude of the ridge of the low-frequency wave m at latitude 56° S after the phase-shifting transformation. Q_m^{new} can be chosen to be any longitude because the geographical locations of ridges or troughs of the waves have no relevance in the moving frames. In this study, we have simply set $Q_m^{\text{new}} = 0$ for all m. $R_m(t)$ is a randomizer which can have values of (0, 1, 2, 3) for $m = 4$, or (0, 1, 2) for $m = 3$, or (0, 1) for $m = 2$, or 0 for $m = 1$. The equiprobable values of $R_m(t)$ are determined by a random number generator. The randomizer used here is to select randomly but with an equal possibility the m possible positions for the moving frame that follows the low-frequency wavenumber m.

Critical to the success of the phase-shifting technique is that the zonal asymmetries in the time-mean maps of a phase-shifted field are free from the zonal asymmetries of the same field in the geographically fixed coordinate system. Obviously, panels (a) and (c) of Figs. 7–10 always meet this criterion because we have removed the stationary waves in these two fields prior to applying the phase-shifting technique to these fields. However, the question whether the zonal inhomogeneity in panel (b) of these figures could only consist of traveling storm tracks cannot be answered easily since we cannot remove the stationary storm tracks prior to the phase-shifting technique (the storm tacks are mathematically defined in terms of the time-mean of a second moment and positive definite quantity).

Intuitively, it is reasonable to argue that the zonally inhomogeneous part of the rms field observed in the geographically fixed coordinate system (e.g., Fig. 1b) would become zonally uniform in a moving frame provided that the phase-shifting method produces little or no longitudinal bias. To validate this intuitively-oriented criterion, we plot in Fig. 13(i) the histograms of the position of the first ridge east of 0° longitude of a low-frequency wave m in 500 mb geopotential height at 56° S as a function of 5°/m degree-wide longitude boxes from 0° to 360°/m for $m = 1$ through 4 (bars), and (ii) the amplitude of the corresponding wave averaged over all cases when its ridge is in the same longitude box (curves). A perfect lack of preference in any longitudinal sectors of a moving frame would be indicated by series of bars with the same height and a level curve for the mean amplitude. Obviously, each of the four moving frames fails to produce a purely uniform distribution in longitude for the frequency of occurrences of the ridge (otherwise the height of the bar in each box would be equal to 27.5 = 1980 cases/72 longitude boxes). Nevertheless, the frequency of occurrence of the

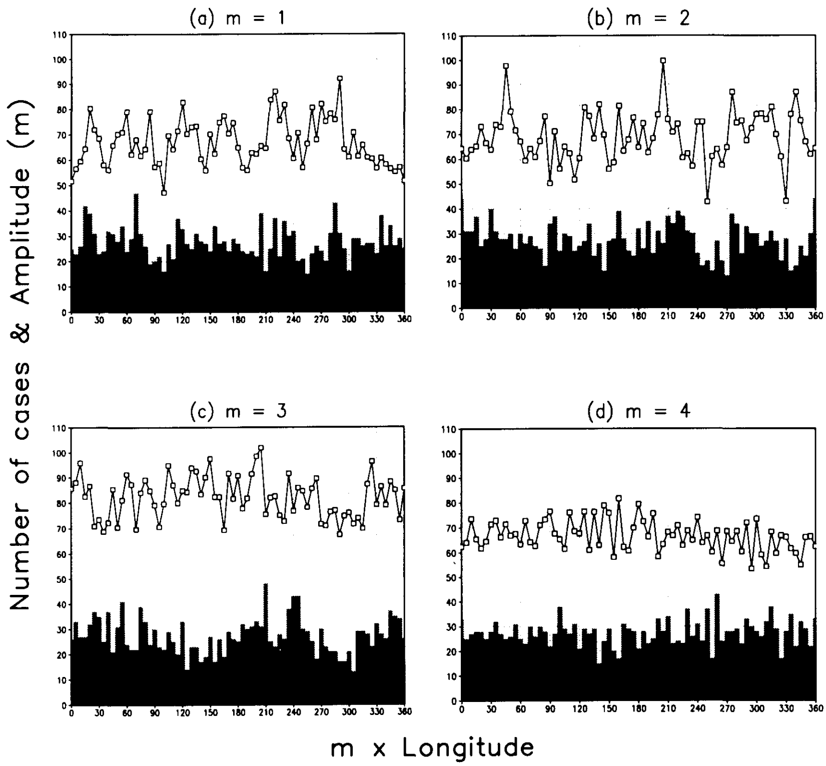

Fig. 13. Histograms of the frequency of occurrence of the ridge position east of Greenwich of a low-frequency wave m at 56° S as a function of longitude box, with width of 5/m degrees. The curve is the amplitude (in unit of meters) of the wave averaged over all of the cases that the ridge occurred in the same longitude box. (a) $m = 1$; (b) $m = 2$; (c) $m = 3$; and (d) $m = 4$. Note that the y-axis represents both the number of the cases (bar) and amplitude (curve).

ridge east of Greenwich is nearly uniform in longitude and more importantly it does not show any coherent preference over any longitude sectors.

We have also performed a series of experiments with the SH dataset parallel to those reported in Section 6 of CD1. The empirical evidence reported in CD1 has been confirmed with the SH dataset, suggesting empirically that the zonal inhomogeneity on a rms map of the phase-shifted high-frequency eddies (i.e., panel (b) in Figs. 7–10) has little signal from the stationary storm tracks. We therefore could attribute the zonal inhomogeneity on such a map to the traveling storm tracks.

REFERENCES

Berbery, E. H., Nogués-Paegle, J. and Horel, J. D. 1992. Wavelike Southern Hemisphere extratropical teleconnections. *J. Atmos. Sci.* **49**, 155–177.

Cai, M. and Mak, M. 1990. Symbiotic relation between planetary and synoptic-scale waves. *J. Atmos. Sci.* **47**, 2953–2968.

Cai, M. and Van den Dool, H. M. 1991. Low-frequency waves and traveling storm tracks. Part I: barotropic component. *J. Atmos. Sci.* **48**, 1420–1436.

Cai, M. and Van den Dool, H. M. 1992. Low-frequency waves and traveling storm tracks. Part II: three-dimensional structure. *J. Atmos. Sci.* **49**, 2506–2524.

Cai, M. and Van den Dool, H. M. 1994. Dynamical decomposition of low-frequency tendencies. *J. Atmos. Sci.* **51**, 2086–2100.

Hansen, A. R. and Sutera, A. 1991. Planetary-scale flow regimes in midlatitudes of the Southern Hemisphere. *J. Atmos. Sci.* **49**, 952–964.

Hartmann, D. L. 1977. Stationary planetary waves in the Southern Hemisphere. *J. Geophys. Res.* **82**, 4930–4934.

Hoskins, B. J., James, I. N. and White, G. H. 1983. The shape, propagation and mean-flow interaction of large-scale weather systems. *J. Atmos. Sci.* **40**, 1595–1612.

Karoly, D. J. 1990. The role of transient eddies in low-frequency zonal variations of the Southern Hemisphere circulation. *Tellus* **42A**, 41–50.

Kidson, J. W. 1988. Interannual variations in the Southern Hemisphere circulation. *J. Climate* **1**, 1177–1198.

Kidson, J. W. 1990. Interseasonal variations in the Southern Hemisphere circulation. *J. Climate* **4**, 939–953.

Lau, N.-C. and Holopainen, E. O. 1984. Transient eddy forcing of the time-mean flow as identified by geopotential tendencies. *J. Atmos. Sci.* **41**, 313–328.

Mo, K. C. and White, G. H. 1985. Teleconnections in the Southern Hemisphere. *Mon. Wea. Rev.* **113**, 22–37.

Newton, C. W. 1972. Meteorology of the Southern Hemisphere. *Meteor. Monogr.* **35**, 263 pp.

Robinson, W. A. 1991a. The dynamics of low-frequency variability in a simple model of the global atmosphere. *J. Atmos. Sci.* **48**, 429–441.

Robinson, W. A. 1991b. The dynamics of the zonal index in a simple model of the atmosphere. *Tellus* **43A**, 295–305.

Sheng, J. and Derome, J. 1991. An observational study of the energy transfer between the seasonal mean flow and transient eddies. *Tellus* **43A**, 128–144.

Simmons, A. J., Wallace, J. M. and Branstator, G. W. 1983. Barotropic wave propagation and instability, and atmospheric teleconnection patterns. *J. Atmos. Sci.* **40**, 1363–1392.

Taljaard, J. J., Van Loon, H., Crutcher, H. L. and Jenne, R. L. 1969. *Climate of the upper air: Southern Hemisphere*, vol. 1. *Temperatures, dew points, and heights at selected pressure levels*. NAVAIR 50-IC-55, Chief of Naval Operations, Washington, DC, 135 pp.

Trenberth, K. E. 1979. Interannual variability of the 500 mb zonal mean flow in the Southern Hemisphere. *Mon. Wea. Rev.* **107**, 1515–1524.

Trenberth, K. E. 1980a. Atmospheric quasi-biennial oscillations. *Mon. Wea. Rev.* **108**, 1370–1377.

Trenberth, K. E. 1980b. Planetary waves at 500 mb in the Southern Hemisphere. *Mon. Wea. Rev.* **108**, 1378–1389.

Trenberth, K. E. 1981. Observed Southern Hemisphere eddy statistics at 500 mb: frequency and spatial dependence. *J. Atmos. Sci.* **38**, 2585–2605.

Trenberth, K. E. 1991. Storm tracks in the Southern Hemisphere. *J. Atmos. Sci.* **48**, 2159–2178.

Trenberth, K. E. 1992. *Global analyses from ECMWF and atlas of 1000 to 10 mb statistics*. NCAR Technical Note NCAR/TN-373 + STR, National Center for Atmospheric Research, Boulder, June 1992, 191 pp.

Trenberth, K. E. and Mo, K. C. 1985. Blocking in the Southern Hemisphere. *Mon. Wea. Rev.* **113**, 3–21.

Trenberth, K. E. and Olson, J. G. 1988. An evaluation and intercomparison of global analyses from the National Meteorological Center and the European Centre for Medium Range Weather Forecasts. *Bull. Amer. Met. Soc.* **69**, 1047–1057.

Van Loon, H. 1965. A climatological study of the atmospheric circulation in the Southern Hemisphere during the IGY, Part I: 1 July 1957–31 March 1958. *J. Appl. Meteor.* **4**, 479–491.

Van Loon, H., Kidson, H. J. and Mullen, A. B. 1993. Decadal variation of the annual cycle in the Australian dataset. *J. Climate* **6**, 1227–1231.

Yu, J.-Y. and Hartmann, D. L. 1993. Zonal flow vacillation and eddy forcing in a simple GCM of the atmosphere. *J. Atmos. Sci.* **50**, 3244–3259.